

# Operating a quantum pump in a closed circuit

Itamar Sela and Doron Cohen

Department of Physics, Ben-Gurion University, Beer-Sheva 84005, Israel

**Abstract.** During an adiabatic pumping cycle a conventional two barrier quantum device takes an electron from the left lead and ejects it to the right lead. Hence the pumped charge per cycle is naively expected to be  $Q \leq e$ . This zero order adiabatic point of view is in fact misleading. For a closed device we can get  $Q > e$  and even  $Q \gg e$ . In this paper a detailed analysis of the quantum pump operation is presented. Using the Kubo formula for the geometric conductance, and applying the Dirac chains picture, we derive practical estimates for  $Q$ .

## 1. Introduction

Understanding of charge transport in mesoscopic and molecular size devices is essential for the future realization of ‘quantum circuits’ [1]. Of particular interest are adiabatic processes that take electrons and move them one by one via a device. The simple minded peristaltic point of view of such process is misleading: such picture looks valid in the case of an open circuit, but breaks down once the pump is integrated into a closed circuit [2, 3, 4]. It is the purpose of this paper to further elaborate on the physics of quantum pumping in *closed circuits*, and to provide a detailed analysis of a prototype pump. The interest and the feasibility of realizing experiments with closed circuits is discussed in Section 1.3 of [5].

### 1.1. The prototype pumping device

The prototype example for a quantum pumping device is the two barrier model (Fig.1). The one particle Hamiltonian is

$$\mathcal{H}(X_1(t), X_2(t)) = \frac{1}{2m} \hat{p}^2 + X_1(t) \delta(\hat{x} - x_1) + X_2(t) \delta(\hat{x} - x_2) \quad (1)$$

where  $m$  is the mass of the particle and  $(\hat{x}, \hat{p})$  are the position and the momentum operators. The region  $x < x_1$  is the left lead, and the region  $x > x_2$  is the right lead. We refer to the segment  $x_1 < x < x_2$  as the “dot region”. The driving is performed by changing  $X_1$  and  $X_2$  in time. In an actual experiment the control parameters  $X_1$  and  $X_2$  represent gate voltages. In order to talk about charge transfer we have to define also a current operator. In what follows we use the conventional definition

$$\mathcal{I} = \frac{e}{2m} (\hat{p} \delta(\hat{x} - x_0) + \delta(\hat{x} - x_0) \hat{p}) \quad (2)$$

where  $e$  is the charge of the particle and  $x_0$  is an arbitrary section point. The momentary current via different sections is in general not the same. But if we integrate it over a whole pumping cycle the result becomes independent of  $x_0$ .

The pumping device can be used in two different configuration. In the case of an *open geometry* (Fig.1) the leads are attached to reservoirs that have the same chemical potentials. For simplicity one assumes a zero temperature Fermi occupation.

In the case of a *closed geometry* (Fig.1) the leads are detached from the reservoirs and are connected together so as to have a ring. This means periodic boundary conditions over a large space interval  $(-L/2) < x < (L/2)$ . Furthermore, the closed system is assumed to be strictly isolated from any environmental influences. The closed system can be regarded as a network with two nodes that are connected by two bonds one of length  $L_D$  (dot region) and the other of length  $L_W$  (wire region). The total length of the ring is  $L = L_D + L_W$ . We assume that  $L_D \ll L$ .

### 1.2. Open (leads) geometry

The *open version* of the two barrier model has been considered in Ref.[6] using the scattering matrix formalism of Büttiker Prêtre and Thomas (BPT) [7, 8]. A typical pumping cycle is illustrated in Fig.2c. In the 1st half of the cycle an electron is taken from the left lead into the dot region via the left barrier, while in the second half of the cycle an electron is transferred from the dot region to the right lead via the right barrier. Naively, by this peristaltic picture, it seems that at most one electron is pumped through the device per cycle. This expectation is supported by the formal calculation. Using the BPT formula one obtains [9]

$$Q = (1 - \bar{g}_T)e \quad (3)$$

where  $0 < \bar{g}_T < 1$  characterizes the transmission of the device during the charge transfer. In the limit  $\bar{g}_T \rightarrow 0$ , which is a pump with *no leakage*, indeed one gets  $Q = e$ . Otherwise one gets  $Q < e$ .

### 1.3. Closed (ring) geometry

Our interest is in the *closed version* of the two barrier model. A major observation is that the pumped charge  $Q$  is *not* “quantized” even if the device is closed and isolated from any environmental influences. Moreover, it can be larger than unit charge. In fact we can have  $Q \gg e$ .

The analysis that we are going to present demonstrates and refines general results that were obtained in Ref.[3]. There we have worked out an artificial circuit which has been modeled as a 3 site system. In the present paper we would like to work out a major prototype model that allows the desired comparison between results for closed circuit as opposed to that of open geometry [Eq.(3)].

We are going to use the Kubo approach to quantum pumping [2, 3, 4]. The “Dirac chains picture” which we further review in the next subsection makes a distinction between “near field” and “far field” pumping cycles. The near field result has been further considered in Ref.[10] using an extension of the BPT scattering approach to quantum pumping.

### 1.4. The Dirac chains picture

In order to analyze an *adiabatic* [11] pumping cycle we have first to understand the geometry of the parameter space. In fact the parameter space of the two barrier model is three dimensional  $(X_1, X_2, X_3)$  where  $X_3 = \Phi$  is the flux via the ring. In

practice we assume a planar  $\Phi = 0$  pumping cycle, but for the theoretical discussion it is convenient to regard  $\Phi$  as a free parameter.

We ask what is the amount of charge which is transported via a section of the ring per cycle. For this purpose we have to calculate the current  $I = \langle \mathcal{I} \rangle$  at each moment. If we were changing the flux we would have by Ohm law  $I = -G^{33}\dot{\Phi}$  where  $G^{33}$  is called the Ohmic (dissipative) conductance. But if we change (say) the parameter  $X_1$  then  $I = -G^{31}\dot{X}_1$ , where  $G^{31}$  is called the geometric (non-dissipative) conductance [12, 13, 14]. In general we can write  $dQ = -G^{31}dX_1 - G^{32}dX_2$  and hence

$$Q = \oint Idt = \oint \mathbf{G} \cdot d\mathbf{X} \quad (4)$$

where  $\mathbf{X} = (X_1, X_2)$  and  $\mathbf{G} = (G^{31}, G^{32})$ .

The elements of the conductance matrix  $G^{kj}$  can be calculated using the Kubo formula. It turns out [11, 14] that in the adiabatic limit  $G^{31} = B_2$  and  $G^{32} = -B_1$  where  $\vec{B}$  is the “magnetic” field (2-form) which appears in the theory of Berry phase [11]. The sources of this field are Dirac monopoles that are located at the points of degeneracy. For the double barrier model a given level  $n$  can have a degeneracy provided  $X_1 = X_2$ , and either  $\Phi = 0$  or  $\Phi = \pi\hbar/e$  modulo  $2\pi\hbar/e$ . In fact we have for each level (excluding the ground state) two Dirac chains of degeneracies as in Fig.2d.

From the above observation one easily draws the following conclusions: (i) We can get  $Q \gg e$  for a tight cycle around a Dirac chain if the degeneracy is in the pumping plane. (ii) We can get  $Q \ll e$  for a tight cycle around a Dirac chain if the degeneracy is off the pumping plane. (iii) We can get  $Q \sim e$  for a cycle which is located in the far field of a Dirac chain. The existence of a far field region is not self evident. This constitutes a major motivation for the present study.

### 1.5. outline

The outline of this paper is as follows. In section 2 we clarify the starting point of the calculation, which is the Kubo formula. In section 3 we introduce a preliminary discussion of the expected results and their significance. Then in sections 4 to 11 we analyze the pumping process in the two barrier model. In particular we find the dependence of  $Q$  on the “radius” of the pumping cycle, and make a distinction between “near field” and “far field” results.

## 2. The Kubo formula

Given a time dependent Hamiltonian  $\mathcal{H}(X)$  with  $X = X(t)$  we define  $\mathcal{F} = -\partial\mathcal{H}/\partial X$  and would like to calculate the generalized conductance as defined by the expression

$$\langle \mathcal{I} \rangle = -G \dot{X} \quad (5)$$

We label by  $n$  the adiabatic levels of the closed ring. The adiabatic states are defined by the equation  $\mathcal{H}|n\rangle = E_n|n\rangle$  with implicit  $X$  dependence. Using these notations the Kubo formula for the *geometric conductance* can be written as

$$G = \sum_{m(\neq n)} \frac{2\hbar\mathcal{F}_{mn}}{(E_m - E_n)^2} \text{Im}[\mathcal{I}_{nm}] \quad (6)$$

The above expression assumes that only one level ( $n$ ) is occupied. If several levels are occupied we have to sum over them. If we have more than one control variable, say

$X_1$  and  $X_2$ , then we have to use the more elaborated notation  $G^{31}$  and  $G^{32}$  in order to distinguish between different elements of the conductance matrix.

If the pumping cycle crosses very close to a degeneracy, we can get from Eqs.(5-6) a very large current  $I$ , and upon integration we can find that the transported charge is  $Q \gg e$ . In the next sections we shall develop actual estimates for  $Q$ . But first we would like to further illuminate the significance of  $Q$ .

The Schrodinger equation can be written in the *adiabatic basis*, where the *transformed* Hamiltonian matrix takes the form  $H_{nm} = E_n \delta_{nm} + \dot{X} A_{nm}$ , where  $E_n$  are called the adiabatic energy levels, and  $A_{nm}$  is a matrix that can be calculated using a well known recipe (which is summarized in section III of [3]). One regards  $\dot{X}$  as the “small parameter”. If the system is prepared an instantaneous *adiabatic* state  $|n\rangle$ , then the instantaneous current is  $I = 0$ , whereas if it is prepared in an instantaneous *steady* state (an eigenstate of  $H_{nm}$ ), then the instantaneous current is finite, say  $I = I_0$ . Accordingly one can question the physical relevance of  $Q$ : After all typically the initial preparation is an adiabatic state, and not a steady state.

So let us consider an actual physical scenario. For simplicity we assume that only two adiabatic levels are involved: The occupied level  $n$  and next (empty) level  $m = n+1$ . To make the dynamical picture simple we use an analogy with the dynamics of a spin 1/2 particle, and consider the illustration in Fig.3. We regard the state  $n$  as spin polarized in the  $z$  direction, and the state  $m$  as spin polarized in the  $-z$  direction. The instantaneous steady states of the Hamiltonian are polarized along an axis that has a small tilt relative to the  $z$  direction.

Initially the spin is polarized in the  $z$  direction and therefore  $I(t=0) = 0$ . For some time we have  $|X(t) - X(0)| \ll \delta X_c$  where  $\delta X_c$  is the relevant parametric scale for the variation of the adiabatic levels. During this time interval the tilt angle is approximately constant. The spin is performing a precession around the tilted axis. As a results we get  $I(t) \neq 0$ . In fact the maximum current is  $I(t) = 2I_0$ . We get this current after half period of precession.

So we have a modulated current  $I(t)$  that equals upon averaging  $I_0$ . As long as  $|X(t) - X(0)| \ll \delta X_c$  the precession goes on as described above. But on larger time scales we have to take into account the variation in the tilt angle. Consequently the modulation of the current is no longer in the range  $0 < I(t) < 2I_0$ , but rather it is shifted and may increase. Still the average stays approximately  $I_0$ .

Thus we see that in the actual physical scenario the average over  $I(t)$  is the same as the  $I_0$  of the instantaneous steady state. The validity conditions for this statement are essentially the validity conditions of linear response theory, which are further explained in Ref.[3]. The discussion above illuminates the justification for the use of the first order steady state solution of Kubo for the purpose of evaluating the pumped charge in an actual physical scenario.

### 3. Charge transfer during an avoided crossing

The pumped charge  $Q$  is obtained via the integral Eq.(4) using Eq.(6) for  $G$ . On the basis of the naive heuristic picture of the Introduction (and see Fig.2) we expect that most of the contribution to the integral would come from a small segments in  $\mathbf{X}$  space where the *last* occupied level has an avoided crossing with the first unoccupied level. Later we define precisely the region in  $\mathbf{X}$  space where this assumption is a valid approximation.

Let us try to sketch what might come out from the calculation. Later on we are going to do a proper job. But before we dive into the detailed analysis (which is quite lengthy) it would be nice to gain some rough expectation. Given that our interest is focused in a small energy window such that  $E_n \sim E$  we define  $v_E = (2E/m)^{1/2}$ . The mean level spacing in the energy range of interest is

$$\Delta = v_E \frac{\hbar\pi}{L} \quad (7)$$

while the energy splitting  $\Delta_s$  at the avoided crossing might be much smaller. We define the following notations

$$|\mathcal{F}_{nm}| \equiv \sigma_0 \quad (8)$$

$$|\mathcal{I}_{nm}| \equiv \frac{ev_E}{L} \sqrt{g_\varphi} \quad (9)$$

$$\Delta_s/\Delta \equiv \sqrt{1-g_0} \quad (10)$$

where both  $0 < g_\varphi < 1$  and  $0 < g_0 < 1$  are dimensionless. Note that  $g_0$  is related to the overall transmission  $\overline{g}_T$  of the device. The adiabaticity condition is

$$|\dot{X}| \ll \frac{\Delta_s^2}{\hbar\sigma_0} \quad (11)$$

and from Eq.(5) with (6) we get the current

$$\langle \mathcal{I} \rangle = 2 \left( \frac{\hbar\sigma_0}{\Delta_s^2} \dot{X} \right) \left( \frac{ev_E}{L} \right) \sqrt{g_\varphi} \quad (12)$$

The time of the Landau-Zener transition via the avoided crossing is

$$\delta t \approx (\Delta_0/\sigma_0)/\dot{X} \quad (13)$$

and hence the transported charge is

$$Q \approx \langle \mathcal{I} \rangle \delta t \approx \left( \frac{g_\varphi}{1-g_0} \right)^{1/2} e \quad (14)$$

where  $g_0$  and  $g_\varphi$  should be estimated in the region of the avoided crossing. We note that  $g_\varphi/(1-g_0)$  is like the Thouless conductance, and can be regarded as a measure for the sensitivity of the energy levels to a test flux. We have pointed out and discussed this issue in Refs.[2, 3], and later it was derived [10] in the context of the scattering formalism.

In Fig.4 we display the numerically determined  $Q$  for various path segments. The horizontal axis is the  $|X_1 - X_2|$  distance of the path segment from the degeneracy point. As  $|X_1 - X_2|$  becomes small  $g_0 \rightarrow 1$  and we get  $Q \gg e$ . But the asymptotic value  $Q \approx e$  which is observed for large  $|X_1 - X_2|$  cannot be explained by such a simple minded calculation. A major objective of the detailed analysis is to illuminate the observed crossover.

#### 4. The model, basic equations

The one particle Hamiltonian of the two barriers model depends on set of parameters  $(X_1, X_2, \Phi)$ . From now on we use units such that  $e = \hbar = 1$ , and characterize the geometry by the dimensionless parameter

$$b = L_w/L_D \gg 1 \quad (15)$$

We write the wavefunction on the two bonds as:

$$\psi_{\text{dot}}(x) = (2/L)^{1/2} \sqrt{q_D} \sin(\varphi_D(x)) \quad (16)$$

$$\psi_{\text{wire}}(x) = (2/L)^{1/2} \sqrt{q_W} \sin(\varphi_W(x)) \quad (17)$$

where  $\varphi(x) = kx + \text{const}$ . Given  $(X_1, X_2)$  and assuming  $\Phi = 0$ , the eigenstates of this Hamiltonian can be found by searching  $k_n$  values for which the matching conditions on the log-derivatives are satisfied. This leads to the following system of equations:

$$\cot(\varphi_{W1}) + \cot(\varphi_{D1}) = \frac{2m}{k} X_1 \quad (18)$$

$$\cot(\varphi_{W2}) + \cot(\varphi_{D2}) = \frac{2m}{k} X_2 \quad (19)$$

$$\varphi_{D2} - \varphi_{D1} = kL_D \quad (20)$$

$$\varphi_{W2} - \varphi_{W1} = kL_W \quad (21)$$

where it should be clear that  $\varphi_{D1} \equiv \varphi_D(x_1)$  etc. The corresponding eigenenergies are  $E_n = k_n^2/2m$ . A similar system of equation can be written for  $\Phi = \pi$ . We can find the  $q_W/q_D$  ratio for a given eigenstate via the matching condition on the wavefunction at either of the two nodes:

$$\sqrt{q_W} \sin(\varphi_W) = \sqrt{q_D} \sin(\varphi_D) \quad (22)$$

where  $(\varphi_D, \varphi_W)$  mean either  $(\varphi_{D1}, \varphi_{W1})$  or  $(\varphi_{D2}, \varphi_{W2})$ . The normalization condition implies that

$$\frac{L_D}{L} q_D + \frac{L_W}{L} q_W \approx 1 \quad (23)$$

For an “ergodic state” we have  $q \approx 1$  for both bonds. In general we characterize an eigenstate by a the mixing parameter

$$\Theta \equiv 2 \arctan \left( \sqrt{\frac{\text{Prob}(\text{wire})}{\text{Prob}(\text{dot})}} \right) = 2 \arctan \left( \sqrt{b} \left( \frac{q_W}{q_D} \right)^{1/2} \right) \quad (24)$$

such that  $\Theta = 0$  means a definite dot state, while  $\Theta = \pi$  means a definite wire state. In practice we have  $0 < \Theta < \pi$ .

In the numerical analysis we use units such that  $m = 1$  and  $L_D = 1$ . Given  $X_1$  and  $X_2$  we solve the system of equations for the  $k_n$  and for the  $\varphi^{(n)}$  at the nodes. Then we determine  $q^{(n)}$  at each bond, and from the ratio we get  $\Theta^{(n)}$  as well.

## 5. Regions in $X$ space

We focus on a small energy window such that the energy levels of interest are  $E < E_n < E + dE$ . We characterize a barrier  $X\delta()$  using its transmission

$$g(X) = \left[ 1 + \left( \frac{1}{v_E} X \right)^2 \right]^{-1} \approx \left( \frac{1}{v_E} X \right)^{-2} \quad (25)$$

The last expression holds if  $g(X) \ll 1$ . We can regard  $g_1 = g(X_1)$  and  $g_2 = g(X_2)$  as an alternate way to specify  $X_1$  and  $X_2$ . The  $(X_1, X_2, \Phi)$  space is divided into various regions (Fig.5a). There is a region where  $g_1$  and  $g_2$  are of order one ( $|1 - g| \ll 1$ ). There the delta functions at the nodes can be treated as a small perturbation. There is a region where  $1/b \ll g_1, g_2 \ll 1$ . There each dot level mix with many wire levels.

This intermediate region will be discussed in a future work [15]. Finally there is the region in  $\mathbf{X}$  space which is of interest in the present study:

$$g_1, g_2 \ll 1/b \quad (26)$$

We shall argue that in this region the states are categorized into “wire states” and “dot state”, which mix only whenever the energy level of the dot “cross” an energy level of the wire (Fig.5bcd). This allows to use “two level” approximation in the analysis of the mixing.

The degeneracies of the Hamiltonian occur at points  $(X^{(r)}, X^{(r)})$  along the symmetry axis of  $\mathbf{X}$  space. They are divided into two groups: those that are located in the  $\Phi = 0(\text{mod}(2\pi))$  planes and those that are located in the  $\Phi = \pi(\text{mod}(2\pi))$  planes. In Appendix A we find the explicit expression for  $X^{(r)}$ . It should be clear that each degeneracy point is duplicated  $\text{mod}(2\pi)$  in the  $\Phi$  direction, hence creating what we call a “Dirac chain”.

There are only two non-trivial degeneracies in  $\mathbf{X}$  space which are associated with a given level  $n$ . One is with the neighboring level “from above” and the other is with the neighboring level “from below”.

Once we locate a degeneracy point we can make a distinction between “near field” and “far field” regions. The near field is defined as the region where we can use degenerate perturbation theory in order to figure out the splitting of the levels. In contrast to that, the far field is defined as the region where we can calculate the splitting of the levels by treating the dot-wire coupling as a first order perturbation.

In Fig.5a we show one pumping path that crosses in the near field region, and a second pumping path that crosses in the far field region.

## 6. Eigenstate analysis

In the theoretical analysis it is illuminating to map the behavior of  $k_n$  and  $\Theta^{(n)}$  in  $(X_1, X_2, \Phi)$  space. See Figs.6-7. It is not difficult to realize that the variation of  $\Theta$  is bounded as follows:

$$\sqrt{b} \left[ \frac{1}{4}g \right]^{+1/2} < \tan(\Theta/2) < \sqrt{b} \left[ \frac{1}{4}g \right]^{-1/2} \quad (27)$$

where  $g$  is either  $g_1$  or  $g_2$ . The derivation of this result is as follows: The matching conditions at a given node implies that  $(\varphi_D, \varphi_W)$  are constraint to be on one of two branches which are illustrated in Fig.8. With each point of a given branch we can associate a  $\Theta$  value via Eq.(24) and either Eq.(18) or Eq.(19). It is a straightforward exercise to express  $\Theta$  say as a function of  $\varphi_D$ , and then to find its minimum and maximum values. Assuming that  $g \ll 1$  one obtains Eq.(27).

Given  $\Theta^{(n)}$  we can extract what are the  $q^{(n)}$  at each bond, and what are the  $\varphi^{(n)}$  at the nodes. By solving Eq.(23) with Eq.(24) we get

$$q_D = b (\cos(\Theta/2))^2 \quad (28)$$

$$q_W = (\sin(\Theta/2))^2 \quad (29)$$

then from Eq.(22) with either Eq.(18) or Eq.(19) we find an expression for  $\varphi$  at a given node. In particular we get

$$\varphi_D = \left( 1 \pm \frac{1}{\sqrt{b}} \tan(\Theta/2) + \dots \right) \left[ \frac{1}{4}g \right]^{1/2} \quad (30)$$

Note that  $\varphi$  is well defined mod( $\pi$ ). There are states which are dot-like ( $\Theta \ll 1$ ), and there are states which are wire-like ( $\Theta \sim \pi$ ). There are regions where a dot-like state mix with wire-like state leading to pair of states with  $\Theta^{(+)} \sim \Theta^{(-)} \sim \pi/2$ . From the above formula it follows that in the latter case

$$\varphi_D^{(+)} \approx \varphi_D^{(-)} \approx \left[ \frac{1}{4}g \right]^{1/2} \quad (31)$$

$$|\varphi_D^{(+)} - \varphi_D^{(-)}| = \frac{1}{\sqrt{b}} \left[ \frac{1}{4}g \right]^{1/2} \left( \tan(\Theta^{(+)}/2) + \tan(\Theta^{(-)}/2) \right) \quad (32)$$

## 7. Eigenenergies and "mixing" from perturbation theory

In order to find the splitting and the mixing of the two levels we use perturbation theory once in the far field analysis and once in the near field analysis. In both cases we use the following notations. The unperturbed basis is  $|i\rangle$  with a dot-like state  $|1\rangle$  and a wire-like  $|2\rangle$ . The perturbed eigenstates  $|n\rangle$  are indicated as  $|+\rangle$  and  $|-\rangle$ . The Hamiltonian in both cases has the general form

$$\mathcal{H} = \mathcal{H}_0 + \mathbf{W} = \begin{pmatrix} E_1 & 0 \\ 0 & E_2 \end{pmatrix} + \begin{pmatrix} W_{11} & W_{12} \\ W_{21} & W_{22} \end{pmatrix} \quad (33)$$

The eigenvectors are real so  $W_{12} = W_{21}$ . The Hamiltonian can be written as a linear combination of Pauli matrices

$$\mathcal{H} = \left( \frac{E_1 + E_2}{2} + \frac{W_{11} + W_{22}}{2} \right) \mathbf{1} + \left( \frac{E_1 - E_2}{2} + \frac{W_{11} - W_{22}}{2} \right) \sigma_3 + W_{12} \sigma_1 \quad (34)$$

we define

$$\Delta_s = 2\sqrt{\left( \frac{E_1 - E_2}{2} + \frac{W_{11} - W_{22}}{2} \right)^2 + W_{12}^2} \quad (35)$$

$$\tan(\theta) = \frac{2W_{12}}{(W_{11} - W_{22}) + (E_1 - E_2)} \quad (36)$$

The eigenenergies are

$$E_n = \left( \frac{E_1 + E_2}{2} + \frac{W_{11} + W_{22}}{2} \right) \pm \frac{\Delta_s}{2} \quad (37)$$

The eigenstates are found by rotating a spin half around the  $y$  axis at an angle  $\theta$

$$|+\rangle \longrightarrow \begin{pmatrix} \cos(\theta/2) \\ \sin(\theta/2) \end{pmatrix} \quad (38)$$

$$|-\rangle \longrightarrow \begin{pmatrix} -\sin(\theta/2) \\ \cos(\theta/2) \end{pmatrix} \quad (39)$$

Assuming that the unperturbed basis consists of distinct dot-like and wire-like states, it follows that we can use the following approximation:

$$\Theta^{(+)} = \theta \quad (40)$$

$$\Theta^{(-)} = \pi - \theta \quad (41)$$

Using Eq.(28) and Eq.(32) this implies

$$\sqrt{q_D^{(+)} q_D^{(-)}} \approx \frac{b}{2} |\sin(\theta)| \quad (42)$$

$$|\varphi_D^{(+)} - \varphi_D^{(-)}| = \frac{2}{\sqrt{b}} \left[ \frac{1}{4}g \right]^{1/2} \frac{1}{|\sin(\theta)|} \quad (43)$$



We note that in the strong mixing region we have  $\theta \approx \pi/2$ .

In the next sections we obtain explicit expressions for the “splitting” and the “mixing” using the above scheme. From the numerics (see e.g. Fig.7) we see that these are in fact very satisfactory approximations.

## 8. Far field analysis

The eigenstates of the ring in the  $\mathbf{X}$  region of interest as defined in Eq.(26) can be found using first order perturbation theory with respect to the wire-dot coupling. This is explained below. We have verified numerically that the approximation is remarkable unless we are very close to a degeneracy point. This defines our distinction between “far” and “near” field regions. In the latter case we present in the next section a complementary treatment using degenerate perturbation theory.

The unperturbed Hamiltonian in the far field analysis corresponds to  $X_1 = X_2 = \infty$ . Using the notations as defined in the previous section we take  $|2\rangle$  as the  $n^{\text{th}}$  wire state, and  $|1\rangle$  as the closest dot state from above. Hence

$$E_1 = \frac{1}{2m} \left( \frac{\pi}{L_D} (1 + [n/b]_{\text{integer}}) \right)^2 \quad (44)$$

$$E_2 = \frac{1}{2m} \left( \frac{\pi}{L_W} n \right)^2 \quad (45)$$

Using the formula

$$W_{ij} = -\frac{1}{4m^2 X} [\partial\psi^{(i)}][\partial\psi^{(j)}] \quad (46)$$

we get:

$$W_{11} = -\frac{v_E^2}{2L_D} \left[ \frac{1}{X_1} + \frac{1}{X_2} \right] \quad (47)$$

$$W_{22} = -\frac{v_E^2}{2L_W} \left[ \frac{1}{X_1} + \frac{1}{X_2} \right] \quad (48)$$

$$|W_{12}| = \frac{v_E^2}{2\sqrt{L_D L_W}} \left| \frac{1}{X_1} \pm \frac{1}{X_2} \right| \quad (49)$$

where the  $\pm$  sign in the expression for the dot-wire coupling depends on whether the dot and the wire states have the same parity or not.

In case of a far field pumping cycle we start (say) with very high barriers, and then lower one of them, say  $X_1$ . If we neglected the dot-wire coupling  $W_{12}$ , the dot level would cross the wire level at a point  $X_1 = X^{(n)}$  that can be determined from the equation  $E_1 + W_{11} = E_2$ . At the vicinity of the avoided crossing we obtain

$$|W_{12}| = \frac{1}{2\pi} (bg^{(n)})^{1/2} \Delta \quad (50)$$

where

$$g^{(n)} = \left( \frac{1}{v_E} X^{(n)} \right)^{-2} \quad (51)$$

From the condition  $|W_{12}| \ll \Delta$  we deduce Eq.(26) which defines our  $\mathbf{X}$  region of interest. Furthermore, from the results of the previous section we obtain expressions

for the splitting and for the mixing of the levels:

$$\Delta_s = bg^{(n)} \frac{1}{2L} \|\mathbf{X} - \mathbf{X}^{(r)}\| \quad (52)$$

$$\sin(\theta) = \frac{2}{\sqrt{bg^{(n)}}} \frac{v_E}{\|\mathbf{X} - \mathbf{X}^{(r)}\|} \quad (53)$$

We use the following notation, which we regard as a measure for the distance of the pumping cycle from the nearby degeneracy:

$$\|\mathbf{X} - \mathbf{X}^{(r)}\| = \sqrt{(X_1 - X^{(n)})^2 + \frac{4}{b} \left( \frac{v_E}{\sqrt{g^{(n)}}} \right)^2} \quad (54)$$

The significance of this notation will be further clarified in the next section where we extend the analysis into the near field region.

## 9. Near field analysis

The unperturbed Hamiltonian in the near field analysis corresponds to  $X_1 = X_2 = X^{(r)}$ . We can find a rough approximation for  $X^{(r)}$  using the analysis of the previous section, but in fact we can find the exact expression which is derived in Appendix A, where we also define the obvious notations  $k_r$  and  $g^{(r)}$ . For later calculation the following approximation is useful:

$$X^{(r)} \approx \frac{v_E}{\sqrt{g^{(r)}}} \quad (55)$$

The unperturbed basis consists of the dot-like definite parity state  $|1\rangle$ , and the wire-like definite parity state  $|2\rangle$ . We recall that for these states  $\Theta$  attains its extremal values as remarked at the end of Appendix A. The energies of the unperturbed states are

$$E_1 = E_2 = E_r = \frac{1}{2m} k_r^2 \quad (56)$$

and the perturbation matrix is

$$W_{11} = bg^{(r)} \frac{1}{2L} (\delta X_1 + \delta X_2) \quad (57)$$

$$W_{22} = g^{(r)} \frac{1}{2L} (\delta X_1 + \delta X_2) \quad (58)$$

$$|W_{12}| = \sqrt{b} g^{(r)} \frac{1}{2L} |\delta X_1 - \delta X_2| \quad (59)$$

where

$$\delta X_1 = X_1 - X^{(r)} \quad (60)$$

$$\delta X_2 = X_2 - X^{(r)} \quad (61)$$

Consequently we can determine both the splitting and the mixing of the levels:

$$\Delta_s = bg^{(r)} \frac{1}{2L} \|\mathbf{X} - \mathbf{X}^{(r)}\| \quad (62)$$

$$\sin(\theta) = \frac{2}{\sqrt{b}} \frac{|X_1 - X_2|}{\|\mathbf{X} - \mathbf{X}^{(r)}\|} \quad (63)$$

In the above expression we have extended the interpretation of the distance measure as follows:

$$||\mathbf{X} - \mathbf{X}^{(r)}|| = \sqrt{(X_1 + X_2 - 2X^{(r)})^2 + \frac{4}{b}|X_1 - X_2|^2} \quad (64)$$

Now we realize that the far field results of the previous section are formally a saturated version of the near field results with

$$|X_1 - X_2|_\infty = \frac{v_E}{\sqrt{g^{(n)}}} \quad (65)$$

## 10. The expressions for $G$

We are now ready to calculate  $G$  from Eq.(6). There are of course  $G^{31}$  and  $G^{32}$  but the expressions look alike so we concentrate, say, on the case  $X = X_1$ , and suppress the node indication subscript whenever possible. By definition  $\mathcal{F} = -\partial\mathcal{H}/\partial X = \delta(\hat{x} - x_1)$ . The current operator has been defined in Eq.(2), but we still have the freedom to set  $x_0$  as we want. So the natural choice for sake of calculation, is obviously  $x = x_1$ . We shall expand later on the results that would be obtained if the current were measured via a different section. The matrix elements of the operators involved are

$$\begin{aligned} \mathcal{F}_{nm} &= -\frac{2}{L} \sqrt{q_D^{(n)} q_D^{(m)}} \sin(\varphi_D^{(n)}) \sin(\varphi_D^{(m)}) \\ \mathcal{I}_{nm} &= i \frac{e}{mL} \sqrt{q_D^{(n)} q_D^{(m)}} \left[ \frac{k_n + k_m}{2} \sin(\varphi_D^{(m)} - \varphi_D^{(n)}) + \frac{k_n - k_m}{2} \sin(\varphi_D^{(m)} + \varphi_D^{(n)}) \right] \end{aligned} \quad (66)$$

One should notice that  $\mathcal{F}_{nm}$  is real and symmetric with respect to  $n \leftrightarrow m$  interchange, while  $\mathcal{I}_{nm}$  is antisymmetric and purely imaginary as implied by time reversal symmetry. Once we sum Eq.(6) over all the occupied levels,  $nm$  terms cancel with  $mn$  terms. Within the framework of the “two level approximation” the only remaining term involves the occupied level  $n$  and the next empty level  $m = n + 1$

$$G^{31}(X_1, X_2) = 2 \frac{\mathcal{F}_{nn} \text{Im}[\mathcal{I}_{nn}]}{\Delta_s^2} \quad (67)$$

We recall the following expressions:

$$\sqrt{q_D^{(+)} q_D^{(-)}} \approx \frac{b}{2} |\sin(\theta)| \quad (68)$$

$$\varphi_D^{(+)} \approx \varphi_D^{(-)} \approx \left[ \frac{1}{4} g \right]^{1/2} \quad (69)$$

$$|\varphi_D^{(+)} - \varphi_D^{(-)}| \approx \frac{2}{\sqrt{b}} \left[ \frac{1}{4} g \right]^{1/2} \frac{1}{|\sin(\theta)|} \quad (70)$$

Upon substitution we realize that both in the near and in the far field we can neglect the second term in the expression for  $\mathcal{I}_{nm}$ . Consequently

$$G^{31}(X_1, X_2) = -\frac{1}{4} (gb)^{3/2} \frac{ev_E}{L^2} \frac{1}{\Delta_s^2} |\sin(\theta)| = -\frac{2 ev_E}{b\sqrt{g}} \frac{|X_1 - X_2|}{||\mathbf{X} - \mathbf{X}^{(r)}||^3} \quad (71)$$

We observe that in the near field, where  $||\mathbf{X} - \mathbf{X}^{(r)}||$  is essentially the Euclidean measure of distance, we get the field of a Dirac monopole as expected. But as we go to the far field the  $|X_1 - X_2|$  contribution saturates as explained in the previous section.

### 11. The calculation of $Q$

Having found  $G^{31}$  and a similar expression for  $G^{32}$  we can perform the integration of Eq.(4) in order to obtain  $Q$ . We already pointed out that most of the contribution in the regions of our interest comes from the avoided crossings. In the near field it is most convenient to make the integration along  $X_1 - X_2 = \pm \text{const}$  segments, while in case of the far field we make the integration along  $X_2 = \infty$  and  $X_1 = \infty$  segments.

It is not difficult to realize that in the near field calculation both segments ( $X_1 - X_2 = \pm \text{const}$ ) give the same contribution. This means that we simply have to do one of the integral and to multiply by 2. But in the far field one should be more careful. If we measure the current in the *middle* of the dot (as indeed done in the numerics) then the same rule applies. But if we measure the current (say) at node 1, then the predominant contribution to  $Q$  comes obviously from the  $X_2 = \infty$  segment, so the result should not be multiplied by 2. Performing a straightforward calculation of the  $dX$  integral, using

$$\int_{-\infty}^{+\infty} \frac{dx}{(x^2 + a^2)^{3/2}} = \frac{2}{a^2} \quad (72)$$

and taking the above discussion into account, we get in the near field

$$Q \approx \frac{X^{(r)}}{|X_1 - X_2|} e \quad (73)$$

One can show that this result is in agreement with the rough estimate of Eq.(14). However, in the far field we have to substitute the saturated value of  $|X_1 - X_2|$  leading to the result  $Q \approx e$ .

The calculation in the far field does not care whether the pumping cycle encircle a  $\Phi = 0$  degeneracy or a  $\Phi = \pi$  degeneracy. It is only in the near field of  $X^{(r)}$  that we see the difference. This is clearly confirmed by the numerics (Fig.4). But a closer look reveals that the far field numerical result for  $Q$  is somewhat smaller than 1. This might look like a contradiction with respect to the general expectations. The resolution of this puzzle is related to the limitation of the far field perturbative treatment. Within the framework of this treatment  $\Theta^{(n)}$  changes from  $\Theta^{(n)} = \pi$  to  $\Theta^{(n)} = 0$  as we lower (say) the  $X_1$  barrier. But in fact we know from section 8 that  $\Theta$  is bounded. This means that not all the the probability gets into the dot region. Consequently, if we integrate along the  $X_2 = \infty$  segment, we expect to get  $Q < e$  as observed. On the other hand, in case of a full pumping cycle, we have to cross from the  $X_2 = \infty$  segment to the  $X_1 = \infty$  segment. This was neglected in our calculation. Thus if we had a full cycle we would expect to get  $Q \approx e$  in the far field as implied by the Dirac chains picture.

### 12. Discussion

We were able to derive an estimate for  $Q$  in the case where the pumping cycle is dominated by a single degeneracy. Within this framework we can still distinguish between near field (where  $Q \gg e$ ) and far field (where  $Q \sim e$ ) regions. Our results are in agreement with those of Ref.[3]. We note that an optional derivation of the near field limit has been introduced in Ref.[10] using an extension of the BPT scattering formalism. But the latter derivation was not suitable to reproduce the far field result because it has been *assumed* there that the charge cannot accumulate in the dot region.

It should be re-emphasized that the results that we have obtained assume that the pumping cycle is dominated by a single degeneracy. In a follow up work [15] we shall discuss the case where the charge transport involves many levels, such that the contribution of neighboring levels (in Eq.(6)) is negligible compared with contribution that comes from  $|m - n| > 1$  levels.

The results that we obtain for a closed geometry are very different from those that are obtained for an open geometry. This is because the motion of the electron is “recycled”. In a more technical language this means that multiple rounds should be taken into account in the calculation of correlation functions. Refs.[16, 4] further discuss how the Kubo formula can be used in order to interpolate these two extreme circumstances.

It should be clear that adiabatic transport becomes counter-intuitive if one adopts a misleading zero order point of view of the adiabatic process. Moreover, even within the “two level approximation” it would not be correct to say that  $Q$  is determined by *peristaltic* mechanism: namely, it is not correct to say that charge transfer is regulated by the Landau-Zener transitions.

A *peristaltic* mechanism would imply  $Q \sim e$ . In the near field we have  $Q \gg e$  so we do not have such mechanism for sure. This is also reflected by having the same  $I$  at both nodes as discussed in the paragraph of Eq.(73). However, even in the far field, where the peristaltic picture seems natural, we have realized that it is an over simplification: also in the case of a far field cycle a finite fraction of  $Q$  is contributed during the intermediate stages of the pumping cycle.

## Appendix A. Finding the degeneracy points

If system is symmetric ( $X_1 = X_2 = X$ ) then we can distinguish between odd and even states leading to the following eigenvalue equations

$$\cot(kL_D/2) + \cot(kL_W/2) = -\frac{2m}{k}X \quad \text{odd states} \quad (\text{A.1})$$

$$\tan(kL_D/2) + \tan(kL_W/2) = +\frac{2m}{k}X \quad \text{even states} \quad (\text{A.2})$$

As we lower  $X$  we have an exact crossing whenever a dot state crosses a wire state with the opposite parity. We have an avoided crossing whenever a dot state tries to cross a wire state with the same parity. The later becomes an exact crossing if the flux through the ring is half integer.

We can determine the degeneracy points by equating (A.1) with (A.2). This gives  $\sin(kL_W) = -\sin(kL_D)$ . For half integer flux it is convenient to use delta gauge on the middle of the wire, so as to get there  $\pi$  phase jump boundary conditions. This implies that in the above equation we make the replacement  $(kL/2) \mapsto (kL/2) + (\pi/2)$ , hence getting the degeneracy condition  $\sin(kL_W) = +\sin(kL_D)$ . We therefore conclude that we have degeneracies for

$$k_r = \frac{\pi}{L_W - L_D} n_r \quad (\text{A.3})$$

They are categorized into  $\Phi=0$  degeneracies for  $n_r = 1, 3, 5, \dots$  and  $\Phi=\pi$  degeneracies for  $n_r = 2, 4, 6, \dots$ . Their location is  $(X^{(r)}, X^{(r)})$  where

$$X^{(r)} = -\frac{k_r}{m} \cot(k_r L_D) \quad (\text{A.4})$$

Accordingly

$$g^{(r)} = g(X^{(r)}) = \sin^2(k_r L_D) = \sin^2(k_r L_W) \quad (\text{A.5})$$

At a degeneracy point the mixing parameter  $\Theta$  that characterizes the odd and the even states attains the extremal values which are allowed by Eq.(27). This can be verified by deducing  $q_w/q_D$  from Eq.(22) with  $\varphi_D = k_r L_D/2$  for the odd state and  $\varphi_D = (\pi/2) + k_r L_D/2$  for the even state.

### Acknowledgments

D.C. thanks M. Moskalets and M. Büttiker for discussions that had motivated this work, and Y. Oreg for urging clarification of the formal result. We are grateful to T. Kottos, H. Schanz and G. Rosenberg for helpful suggestions and help with the numerical procedure. The research was supported by the Israel Science Foundation (grant No.11/02), and by a grant from the GIF, the German-Israeli Foundation for Scientific Research and Development.

### References

- [1] L.P. Kouwenhoven, C.M. Marcus, P.L. Mceuen, S. Tarucha, R. M. Westervelt and N.S. Wingreen, Proc. of Advanced Study Inst. on Mesoscopic Electron Transport, edited by L.L. Sohn, L.P. Kouwenhoven and G. Schon (Kluwer 1997).
- [2] D. Cohen, cond-mat/0208233 (2002); Solid State Communications **133**, 583 (2005).
- [3] D. Cohen, Phys. Rev. B **68**, 155303 (2003).
- [4] For a mini-review see: D. Cohen, Physica E 28, 308 (2005).
- [5] G. Rosenberg and D. Cohen, cond-mat/0510289, J. Phys. A (2006, in press).
- [6] Y. Levinson, O. Entin-Wohlman and P. Wolfle, cond-mat/0010494.
- [7] M. Büttiker, H. Thomas and A. Pretre, Z. Phys. B-Condens. Mat., **94**, 133 (1994).
- [8] P. W. Brouwer, Phys. Rev. B **58**, R10135 (1998).
- [9] T. A. Shutenko, I. L. Aleiner and B. L. Altshuler, Phys. Rev. **B61**, 10366 (2000).
- [10] M. Moskalets and M. Büttiker, Phys. Rev. B **68**, 161311(R) (2003).
- [11] M.V. Berry, Proc. R. Soc. Lond. A **392**, 45 (1984).
- [12] D. J. Thouless, Phys. Rev. B **27**, 6083 (1983).
- [13] J.E. Avron, A. Raveh and B. Zur, Rev. Mod. Phys. **60**, 873 (1988).
- [14] M.V. Berry and J.M. Robbins, Proc. R. Soc. Lond. A **442**, 659 (1993).
- [15] I. Sela and D. Cohen, in preparation.
- [16] D. Cohen, Phys. Rev. B **68**, 201303(R) (2003).

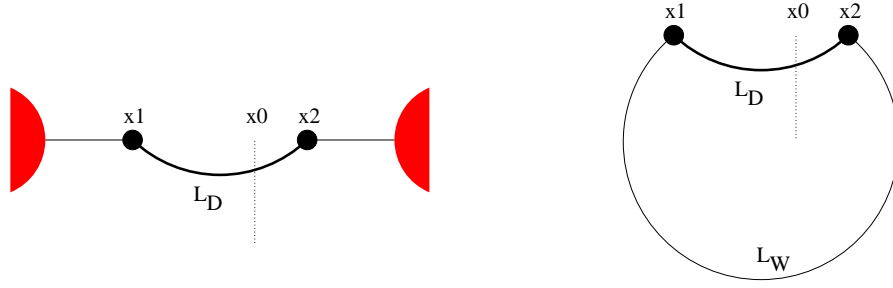


**FIG. 1.** Illustration of the model system. The two barrier pumping device is used in two different configurations. Left panel: open lead geometry; Right panel: closed ring geometry. The barriers are located at the nodes  $x_1$  and  $x_2$  while the current is measured through the section at  $x_0$ .

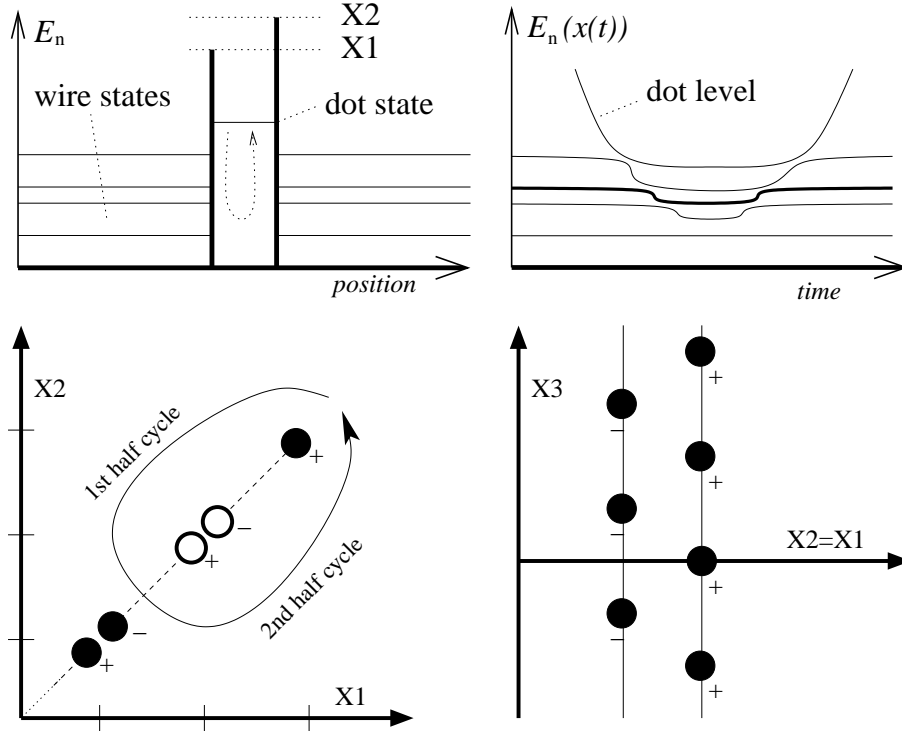


**FIG. 2.** (a) Upper left: The energy levels of a ring with two barriers, at the beginning of the pumping cycle. It is assumed that the three lower levels are occupied. (b) Upper right: The adiabatic levels as a function of time during the pumping cycle. (c) Lower Left: The  $(X_1, X_2)$  locations of the Dirac chains of the 3 occupied levels. Filled (hollow) circles imply that there is (no) monopole in the pumping plane. Note that for sake of illustration overlapping chains are displaced from each other. The pumping cycle encircles 2 + 1 Dirac chains that are associated with the 3rd and 2nd levels respectively. (d) Lower right: The 2 Dirac chains that are associated with the 3rd level.

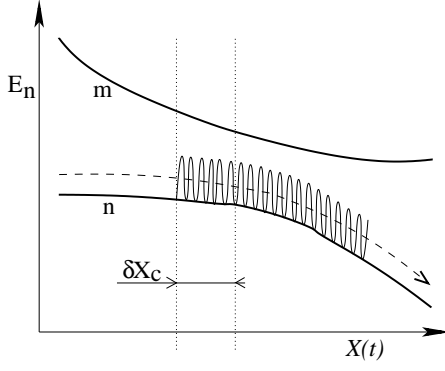


**FIG. 3.** Cartoon of the adiabatic evolution within the framework of the two level approximation. The system is prepared in level  $n$ , and the nearby empty level is  $m = n + 1$ . The control parameter  $X(t)$  is being changed slowly, and therefore the system “oscillates” around the first order adiabatic solution. The energy of the latter is illustrated by a dashed line. Note that the identity of the adiabatic state changes gradually, and can be regarded as constant only on scales  $\delta X \ll \delta X_c$ .

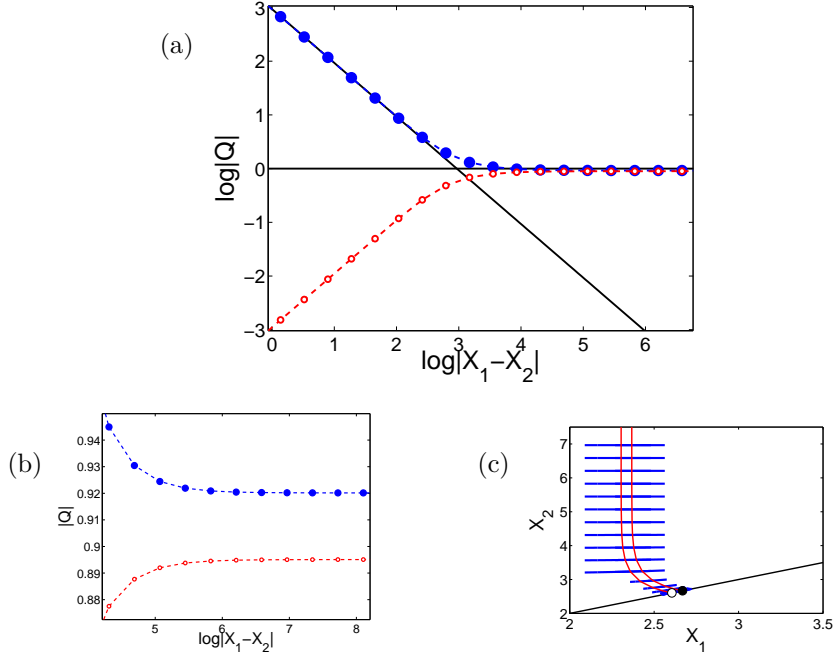


**FIG. 4.** Panels (a) and (b): Numerical calculation of the pumped charge  $Q$ . The model parameters are  $L_D = m = e = 1$  and  $L_W = 3000.43$ . The current  $I$  is measured at the middle of the dot. The numerical integration is carried out along the segments which are indicated in panel (c), and the results are multiplied by 2 so as to include the equal contribution that comes from the second half of the cycle. There are two sets of data points. One set (filled circles) is for pumping cycles that encircle an in-plane degeneracy point ( $n_r = 2993$ ). A second set (hollow circles) is for pumping cycles that encircle an off-plane degeneracy point ( $n_r = 2992$ ). The location of the avoided crossing for each data set is indicated by the solid lines in panel (c). The near and that far field approximations that we derive for  $Q$  are indicated by the solid lines in panel (a). The zoom in panel (b) reveals that  $Q$  in the far field is in fact slightly less than 1, which is explained in section 13.



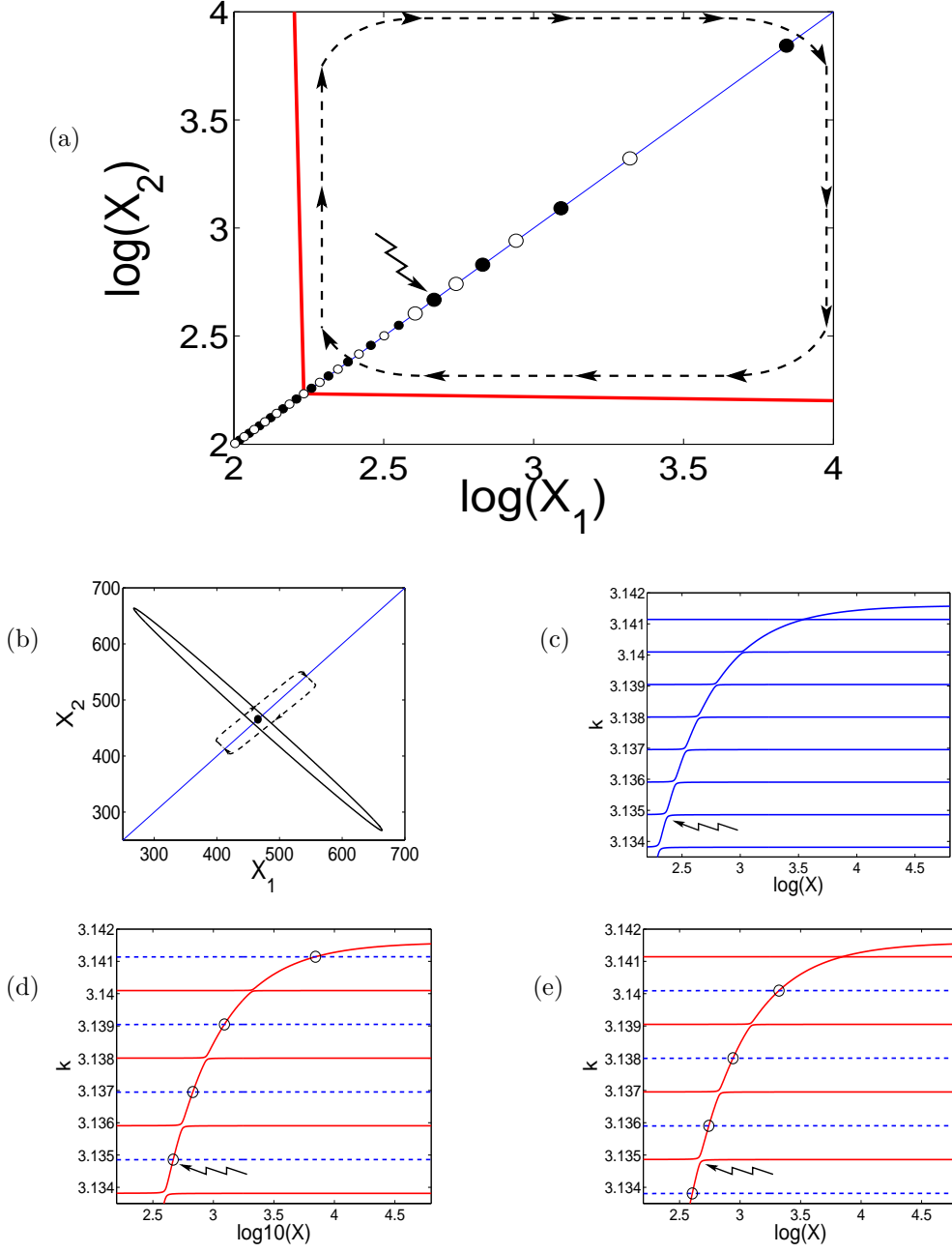


**FIG. 5.** Regions in  $\mathbf{X}$  space. The model parameters are the same as in the previous figure. Panel (a) displays the region of interest as defined in Eq.(26). It is bounded by the left and by the bottom solid lines which are defined by  $g(X) \sim 1/b$ . In-plane and off-plane degeneracy points are indicated by filled and hollow circles respectively. We indicate by arrow one in-plane degeneracy point ( $n_r = 2993$ ). A zoom of its near field is displayed in panel (b). The ellipse in panel (b) indicates a level splitting that equals  $\Delta/10$ . The dashed lines in panels (a) and (b) indicate far field and near field pumping cycles respectively. In panels (c)-(e) we show the energy levels ( $k_n$ ) along three paths in  $\vec{X}$  space, which are  $(X_1=X, X_2=\infty, \Phi=0)$ , and  $(X_1=X, X_2=X, \Phi=0)$ , and  $(X_1=X, X_2=X, \Phi=\pi)$  respectively. The degeneracies  $n_r = 2992 \dots 2999$  are circled. The arrow indicates the representative degeneracy point  $n_r = 2993$ . In panels (d) the odd states are indicated by dashed lines so as to distinguish them from the even states.

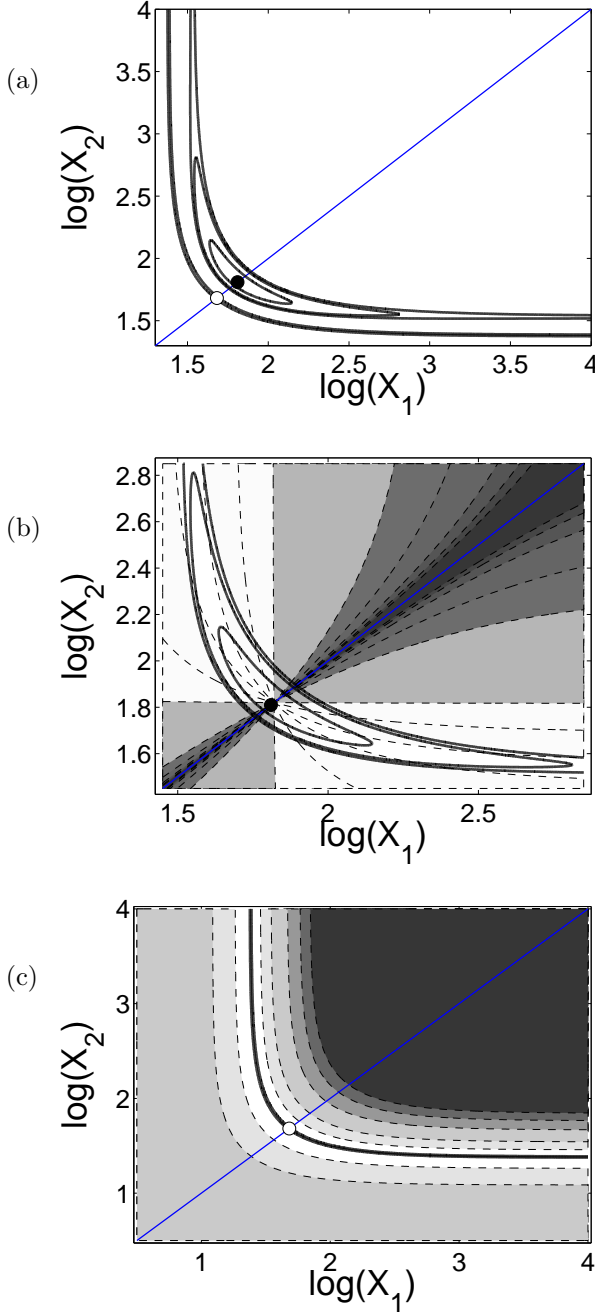


**FIG. 6.** The energy level splitting and the mixing parameter  $\Theta$  for two pairs of levels. The model parameters are  $L_D = m = e = 1$  and  $L_W = 160.43$ . In panel (a) we show the contour lines for the energy level splitting of the first (even) dot level with an odd wire level ( $n = 158$ ), and for the energy level splitting of the first (even) dot level with an even wire level ( $n = 157$ ). The two cases are displayed again in panels (b) and (c) respectively where we plot both level splitting contours (solid lines) and  $\Theta$  contours (dashed lines). In the “even-odd crossing” case we have an in-plane degeneracy, which is indicated by a filled circle, while the inner most contour line is for  $\Delta/5$  splitting. Note that within the white regions the mixing is maximal ( $\Theta \sim \pi/2$ ). In the “even-even avoided crossing” case the projection of the off-plane degeneracy point is indicated by a hollow circle.

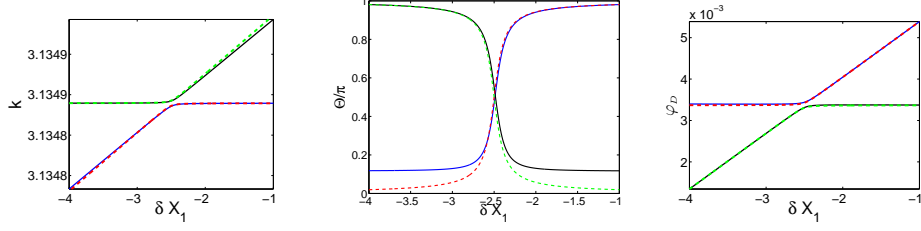


**FIG. 7.** Tests of the perturbation theory based approximations (dashed lines) against the numerics (solid lines). The model parameters are  $L_D = m = e = 1$  and  $L_W = 3000.43$ , and we focus on the degeneracy point  $n_r = 2993$ . For these parameters  $X^{(r)} \approx 465$  and  $g^{(r)} \approx 4.5 \times 10^{-5}$ . All the plots refer to the path  $(X_2 - X_1) = 5$ . In the left panel the dashed lines are derived from Eq.(37). In the middle panel the dashed lines are based on Eqs.(40-41) with  $\theta$  from Eq.(36). In the right panel the dashed lines are deduced from Eq.(30)

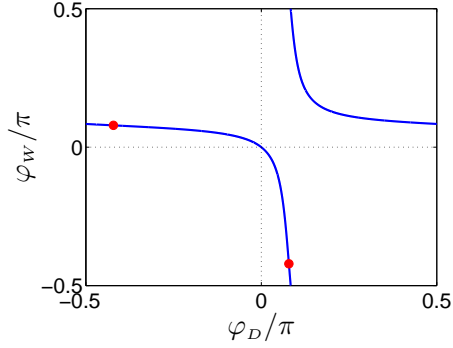


**FIG. 8.** The wire phase  $\varphi_W/\pi$  versus the dot phase  $\varphi_D/\pi$  at a node with delta barrier  $g(X) = 0.225$ . The two branches are implied by the matching condition Eq.(18). The ratio  $|\sin(\varphi_D)/\sin(\varphi_D)|$  attains its extremal values (Eq.(27)) at the points which are indicated by circles.